Improving the structural and transport properties of Cadmium ferrites with the addition of cerium for high frequency applications

Muhammad Akram[a], Saman Akhlaq[a], Muhammad Imran Arshad [b,d,e*], Nasir Amin[b], Ahmad A. Ifseisi[c], Maria Akhtar[b], Le Duc Tung[d,e], Nguyen Thi Kim Thanh[d,e,*], Nicola Morley[f], Sania Sadiq[a], Safdar Hussain[a], Muhammad Zahid Ishaque[a], Yasir Zaman[a], Atta Ur Rehman[b***],

[a]*Department of Physics, University of Sargodha, 40100, Pakistan*
[b]*Department of Physics, Government College University, Faisalabad, Pakistan.*
[c]*Department of Chemistry, College of Science, King Saud University, P.O. Bo x 2455, Riyadh, 11451, Saudi Arabia.*
[d]*Biophysics Group, Department of Physics and Astronomy, University College London, Gower Street, London, WC1E 6BT, UK.*
[e]*UCL Healthcare Biomagnetics and Nanomaterials Laboratories, 21 Albemarle Street, London W1S 4BS, UK*
[f]*Department of Materials Science and Engineering, The University of Sheffield, UK, S1 3JD.*

Corresponding Author: * ntk.thanh@ucl.ac.uk

**muhammad.arshad@ucl.edu.pk; miarshadgcuf@gmail.com;

***attaurrehman423@gmail.com

Abstract

Due to their outstanding properties, low cost, and environmental friendliness, mixed transition metal oxides are frequently used in various applications. In this study, Ce^{3+} doped $CdFe_2O_4$ powder samples were prepared through the co-precipitation process. A peak shift was observed towards a lower 2θ angle with the substitution of Ce^{3+} at their lattice site and the lattice constant has a maximum value for the $x = 0.06$ sample with the crystallite size of 34 nm. Moreover, for $x = 0.06$ sample, the resistivity was found in the order of 10^6 **Ω** cm and the dielectric tangent loss had a smaller value. The electrical and dielectric analysis of the as-prepared $x = 0.06$ sample indicate that it is the best for high-frequency applications.

Keywords: co-precipitation; crystallite size; resistivity; dielectric; high frequency.

1 Introduction

Spinel ferrites (SFs) have been found to provide applications in various technological fields due to their good response to electromagnetic properties [1]. The dielectric and electrical properties of SFs are based on the electron hopping mechanism between cations. The concentration of doped elements in ferrites causes structural change and affects the conduction process of electrons [2]. The active catalyst of ferrites is used in the selective oxidation of

styrene [3]. Recent research in SFs focused on their biomedical applications like magnetic resonance contrast imaging, targeted drug deliveries, and hyperthermia [4]. Some mixed SFs were used in communication device fabrications for the suppression of electromagnetic radiations to shield interference effects [5]. SFs gas sensors have been made for their high surface response [6]. SFs are extensively used materials in various fields of electronic engineering and telecommunication. Their low cost, durability, chemical and mechanical stability, low hysteresis loss, high resistivity, and good optical, and surface response have made them a good material for various applications. SFs are also playing a role as artificial enzymes in biomedical applications, chemical and food industries [7].

Lanthanide-doped SFs are used in dyes and pigments to produce glazes for their nontoxicity and high-temperature stability as compared to metallic pigments [8]. Another approach of doping the rare earth (RE) elements in spinel ferrites have been adopted, as the lattice parameter change with doping RE elements, thus a change is observed, and used for a variety of application including magnetic recording media, security, switching and high-frequency applications [9].

Induction heat studies are carried on cobalt ferrites for use in hyperthermia applications, for the treatment of cancer with energy obtained from hysteresis energy loss [10]. The grain size, crystallinity, chemical composition, concentration of doped elements, and specific interstitial site occupancy of cations define the properties of ferrites. Moreover, different synthesis conditions like pH value, sintering temperature, and concentration of elements play a vital role in tailoring the electromagnetic, structural, optical, and thermal properties of SFs. Nikumbh *et al*., [11] prepared $Cd_{1-x}Co_xFe_2O_4$ ferrites using the co-precipitation (CP) route. The lattice constant decreased with increasing cobalt doping. This is due to the result of the replacement of a larger Cd^{2+} ion (1.03 Å) by a smaller Fe^{3+} ion (0.63 Å) at the tetrahedral site. Electrical conductivity measurements showed high conductivity of the compound due to the presence of large number of cobalt. Bhongale *et al*., reported the impact of magnesium in cadmium ferrite ($Mg_xCd_{1-x}Fe_2O_4$) prepared by the oxalate CP synthesis route [12]. The prepared doped samples could be used for microwave applications. Saturation magnetization and magnetic moment values depended on the Mg^{2+} ion concentrations. A study was made by Ateia *et al*., [13] on rare-earth (RE) doped Cd-Co ferrites fabrication *via* the sol-gel auto combustion (SGAC) process. The crystallite size of the Ce^{3+} doped Cd-Co sample was 27 nm and the lattice constant was 8.4271 Å.

The purpose of this work was to prepare the $CdCe_xFe_{2-x}O_4$ (Ce-CF) samples (x = 0.0, 0.02, 0.04, 0.06, 0.08, 0.1) and to discuss how the small crystallite size, high resistivity, and a

large dielectric constant along with low dielectric tangent loss can be used for frequency applications. Numerous methods were used so far for SFs preparation including the SGAC process [14-17], co-precipitation (CP) route [18-20], solid-state reaction method [21], and so forth. However, the CP method was used for the synthesis of our samples due to its effectiveness in producing ferrites.

2 Experimental details

2.1 Preparation of cerium Ce^{3+} doped cadmium ferrites

$CdCe_xFe_{2-x}O_4$ (x = 0, 0.02, 0.04, 0.06, 0.08, 0.1) SFs were obtained *via* the co-precipitation method. The precursors were taken in the form of hydrated solid nitrates including Ce $(NO_3)_3.6H_2O$, Cd $(NO_3)_2.4H_2O$, and Fe $(NO_3)_3.9H_2O$. The aqueous solution of all the precursors was made with different concentrations having a molarity value of 0.4 M and thoroughly mixed with magnetic stirring to form a clear solution. NaOH was used as a precipitating agent with a molarity of 1.8 M. At room temperature (RT), the reagent (NaOH) was added with constant stirring to the solution to obtain the metal hydroxides. To get a homogeneous solution, the mixed solution of nitrates and NaOH was stirred for 30 min at RT. Then the temperature was raised to 70 ^oC to proceed with further reaction that leads to the formation of ferrites. The temperature was maintained for 45 min under continuous stirring at a faster rate to avoid any agglomeration. A pH ~ 12 was maintained in the solution during the reaction. The obtained product was washed many times with deionized water to eliminate the contaminants. The sample was then kept in a heating oven and dried at 98 ^oC for 24 h. The dried samples were ground to a fine powder and sintered at 800 ^oC for 8 h.

2.2 Characterization

Bruker D8 Advance X-ray diffractometer was used for X-ray diffraction (XRD) patterns, to investigate the structure of the as-prepared powder samples. Model 2401, Keithley Electrometer was used to measure the current-voltage (I-V) plots to find the electric parameters. The dielectric parameters were recorded using IM3533, LCR Meter.

3 Results and discussion

3.1 Structural analysis

Fig. 1(a) represents sharp peaks XRD pattern for Ce-CF samples and plans (220), (104), (311), (222), (400), (422), and (511) show Miller indices represent spinel phase matrix. A small shift of peaks towards a lower angle with the increasing dopant Ce^{3+} in the $CdFe_2O_4$ lattice is depicted in Fig. 1(b). The extra peaks of CeO_2 [22, 23] are denoted by a mark (*), as depicted in Fig 1(a). The lattice constant (a) and unit cell volume (V) were determined *via* equations:

$$a = d\sqrt{h^2 + k^2 + l^2} \quad (1)$$

$$V = a^3 \quad (2)$$

The lattice constant and unit cell volume (as seen in Table 1) were increased with an increasing Ce^{3+} doping. It is attributed to the replacement of Fe^{3+} ions by Ce^{3+} ions [24, 25]. As the ionic radii of dopant element Ce^{3+} are 1.034 Å and Fe^{3+} is 0.645 Å, therefore the addition of Ce^{3+} expands the lattice, and no further increase was observed in the lattice constant for x = 0.08 to x = 0.1. This behaviour may be attributed to the distortion in lattice caused by the Ce^{3+} ions of larger ionic radii as their solubility in Cd ferrite decreases with a further increase in Ce^{3+} concentration [26]. The crystallite sizes (D) obtained from the Scherrer relation: $D = \frac{n\lambda}{\beta Cos\theta}$ [27] are reported in Table 1. For the pure CF sample, "D" was 40 nm, and as the doping of Ce^{3+} increases the crystallite size reduces from 45 nm to 25 nm. Fig. 1(c) represents the graphical relation of Ce^{3+} with the "a" and "D". The reduction of "D" is attributed to a weaker Fe–O bond as compared to a stronger Ce–O bond [28].

The X-ray density ($\rho_x = \frac{8M}{N_A a^3}$) was improved with a rise in cerium contents and it may be attributed atomic weight of dopant cerium (Ce^{3+}) ions is higher than iron (Fe^{3+}) ions (as seen in Table 1). Moreover, the bulk density ($\rho_m = \frac{Mass}{Volume} = \frac{M}{\pi r^2 \times h}$) indicates a decreasing trend with increasing dopant (as reported in Table 1), which may be due to the expansion of the crystal lattice as a consequence of an enlarged lattice constant and lesser grain growth attributed to the formation of an extra secondary phase at the grain boundary. The variation of "ρ_x" and "ρ_m" with dopant concentration (x) in Ce-CF samples are shown in Fig. 1(d). The expansion of the lattice and formation of bubbles by restricted grain growth caused the drop in measured density (ρ_m) [29].

The porosity percentage (P % = $[1 - \frac{\rho_x}{\rho_m}] \times 100$) was calculated [18] (as reported in Table 1) and the porosity percentage of the Ce-CF powder samples increases with dopant up to x = 0.06 and after that, there was a decrease in P (%). This trend is inconsistent with the values of the "a" as the replacement of Ce^{3+} caused an increase in lattice constant which is responsible for lattice expansion and causing the rise of porosity in the crystal geometry of cadmium ferrites [30]. The change in porosity with cerium content is depicted in Fig. 1(e). The hopping lengths of the tetrahedral (A) site ($L_A = \frac{a\sqrt{3}}{4}$) and octahedral ($B$) site ($L_B = = \frac{a\sqrt{2}}{4}$) show a substantial role in the electrical conduction phenomenon between consecutive cationic sites and are given in Table 1. The increase in the hopping lengths with Ce^{3+} doping up to x = 0.06

was observed. This increase in hopping lengths is in accordance with the expansion of lattice constants with the Ce^{3+} ions of larger radii as compared to Fe^{3+} ions [31]. Further, the increase of Ce^{3+} contents caused a decrease in hopping lengths because of the creation of the impurity phase at grain boundaries and restricting the expansion of the lattice [32]. The values of hopping lengths calculated for all cerium concentrations are shown in figure Fig. 1(f). The number of dislocations (defects) per unit volume of the crystal lattice is known as dislocation density (δ) and is calculated using: $\delta = 1/D^2$. The dislocation density was revealed opposite as compared to crystallite size and is reported in Table 1 for Ce-CF samples. According to the estimated data in Table 1, the "δ", when compared to the pure sample, reaches its highest value at $x = 0.1$, and the sample has better crystallinity when the dislocation line density is smaller.

3.2 Electrical analysis

To study the electrical properties of Ce-CF samples, the two-probe technique for resistivity measurement was adopted. The values of current-voltage (I-V) were recorded in the temperature range 318 K-738 K. Fig. 2(a) revealed temperature *versus* resistivity for different dopant concentrations (x) for Ce-CF ferrite samples. The DC resistivity (ρ) of Ce-CF ferrites decreases with increasing temperature (as seen in Fig. 2(a)). The "ρ" of the un-doped sample was of the order $10^7\ \Omega$ cm at 318 K while the resistivity of doped samples was seen to have the value of the order $10^6\ \Omega$ cm and decreased with the increase of Ce^{3+} contents (x) at 318 K. Vervey's hopping mechanism can be used to explain such resistivity behaviour [33]. This process demonstrated that the electron exchange between ferrous (Fe^{2+}) and ferric (Fe^{3+}) ions *B*-sites is the primary cause of the conduction in SFs. The activation energy and the interionic spacing both affect the probability of hopping. When compared to *B*-*B* hopping, the probability of switching between two separate *B*- and *A*-sites is lower. Therefore, for the obvious reason that ferric ions only exist at *A*-sites, and ferrous ions are only formed during their favourable accommodation at *B*-sites, the hopping between *B*- and *A*-sites does not occur. Therefore, another factor contributing to a change in DC resistivity is the imbalance between the cations.

The DC resistivity *versus* cerium concentration at specific temperatures, as depicted in Fig. 2(b), and the resistivity decreases with increasing the level of dopant concentration. The small resistivity values are due to the decrease of the activation energy (E_a) and the increase of conductivity with the increased dopant concentration [34]. The "E_a" of the Ce-CF samples was determined by taking the slope of the log of resistivity *versus* $1/k_BT$ curves as illustrated in Fig. 2(c). The activation energy *versus* Ce^{3+} doping (x) is shown in Fig. 2(d). It was revealed that the minimum activation energy was found at $x = 0.04$. The drift mobility of charge carriers

increased with temperature as their thermal energy improved with the increase of temperature. The plots of drift mobility *versus* temperature are illustrated in Fig. 2(e). The *A*- and *B*- site hopping lengths increase with Ce^{3+} doping up to $x = 0.06$ and then decrease with an increase of Ce^{3+} doping up to $x = 0.1$ as shown in Fig. 1(f). It affects the conduction of charge carriers at both sites. As the hopping lengths increase the values of resistivity decreases but above $x = 0.06$, the hopping lengths decreases so the resistivity also decreases, indicating a rise in conductivity.

3.3 Dielectric analysis

Fig. 3(a) revealed the relationship of the dielectric constant (ε') *versus* log *f* and ε', which reduces with increasing frequency. The ε' has a greater value at low frequency and the variation in ε' for SFs is attributed to the hopping of ions with different valence states of the same element such as Fe^{2+}/Fe^{3+} [35]. Moreover, the high value of the ε' can be attributed to the distorted lattice due to the addition of Ce^{3+} ions having a higher ionic radius causing the atomic polarizability in the crystal lattice [36]. Fig. 3(b) shows the effect of Ce^{3+} concentration on dielectric constants for Ce-CF samples. The ε' has a maximum value for $x = 0.1$. The addition of larger radii of Ce^{3+} ions would produce vacancies and disorders in the crystal structure which may enhance the possibility of ion polarization contributing to the ε'. The number of electric dipoles moment per unit volume increases when a dielectric material is placed in an electric field. Hence the higher the dielectric constant the larger will be the dipole moment per unit volume. Therefore, the sample $x = 0.1$ has a higher dielectric constant and larger dipole moment. The reduction of the ε' maybe due to the creation of an extra phase that causes hindrance of valence exchange between Fe^{2+} and Fe^{3+} [37].

The dielectric tangent loss (tan δ) can be attributed to the loss of energy by the resonance of domain walls. [14]. Fig. 3(c) shows the plots of the tan δ *versus* log *f*. The values of "tan δ" of the as-prepared ferrites represent a reducing trend with an increase of the frequency except for the samples $x = 0.08$ and $x = 0.1$. The replacement of the Fe^{3+} ion by the cerium (Ce^{3+}) has decreased the Fe^{2+} and Fe^{3+} dipoles on the *B*- site resulting in the increased value of the dielectric loss. The creation of the impurity phase at the grain boundary produces hindrance in electron hopping therefore dielectric loss decreases at higher frequencies. Moreover, the reduction in the resonance of domain walls at higher frequencies causes low values of dielectric loss [38]. The impact of cerium concentration on the ε' of the samples is shown in Fig. 3(d). Fig. 3(e) shows the variation of *ac* conductivity (σ_{ac}) with a log *f*. The "σ_{ac}" of all samples was independent of frequency at a lower frequency, showing the dominance of

σ_{ac} but at higher frequencies, σ_{ac} of the samples increases with the frequency of the applied *ac* field. Maxwell–Wagner's double layer model explained the *ac* conductivity in dielectrics. Conduction occurs due to charge carriers hopping between $Fe^{2+} \leftrightarrow Fe^{3+}$, which is small at a lower frequency region and higher frequency conductive grains become active, and conduction increased [38]. The increase in conductivity can be attributed to the decreased hopping lengths at different lattice sites. Moreover, Fig. 3(f) shows the impact of Ce^{3+} on the "σ_{ac}" of the samples, and it was found that there is enhanced *ac* conductivity with the addition of Ce^{3+}. The impedance plots depicted in Fig. 3(g) indicate a decreasing trend of impedance with the frequency. The impedance trend is in agreement with the dielectric behaviour of the sample with frequency. A decrease in impedance with the frequency indicated an increase in the conduction phenomenon [38]. The impedance in the sample decreases with Ce^{3+} concentration, which showed the conduction phenomenon due to conducting grains at higher frequencies. The Cole-Cole plots given in Fig. 4 showed the relation between real and imaginary parts of dielectric components. The Cole-Cole plots indicate the contribution towards conduction in samples due to grain boundaries or conducting grains. The Cole-Cole plots of samples with higher concentrations of Ce^{3+} showed curves at a higher frequency. The semicircles at higher frequency regions indicated that the conduction phenomenon in samples was due to conducting grains at higher frequencies [38].

4. Conclusions

The CP synthesis technique was adopted for the fabrication of Ce-CF ferrite samples. The spinel matrix was found with the help of XRD, and "*D*" decreased with the Ce^{3+} doping. The reduction in the value of DC resistivity with temperature was observed, and the drift mobility was observed to increase with temperature. Activation energies were calculated, which were in the range of 0.02 eV to 0.2 eV. The ε' reduces with increasing frequency, and the tan δ of the as-prepared samples was found to have a minimum value at $x = 0.06$. The σ_{ac} of the samples was found to increase with frequency, and the Cole-Cole plots showed resistance attributed to grains and grain boundaries. The electrical and dielectric properties of sample $x = 0.06$ revealed that it is appropriate for high-frequency applications.

Funds for postdoc

M. Imran Arshad is highly grateful to HEC, Pakistan for giving him opportunity of Postdoc under post doc batch 3 Ref; 3-1/PDFP/HEC/2022(B-3)/2320/02, and University College London (UCL) UK for hosting this fellowship.

Author Statement

Muhammad Akram: Supervision, **Atta Ur Rehman:** Methodology, writing, Editing **Nasir Amin** Validation; **Saman Akhlaq**: Writing-original draft, **Ahmad A. Ifseisi** Resources, **Maria Akhtar** Investigation, **Le Duc Tung**: Review, **Nguyen Thi Kim Thanh**: Data analysis and critical review, **Nicola Maorley**: Review, **Sania Sadiq:** Data Curation, **Safdar Hussain**; Formal analysis, **Muhammad Zahid Ishaque:** Investigation, **Yasir Zaman**: Formal analysis, **Muhammad Imran Arshad** Supervision, Project administration.

Acknowledgement

The authors are grateful to the Researchers Supporting Project number (RSPD2023R669), King Saud University, Riyadh, Saudi Arabia, for the financial support.

References

[1] M. Yousefi, S. Manouchehri, A. Arab, M. Mozaffari, G.R. Amiri, Amighian, Preparation of cobalt–zinc ferrite ($Co_{0.8}Zn_{0.2}Fe_2O_4$) nanopowder via combustion method and investigation of its magnetic properties, Material Research Bulletin, 45 (2010) 1792-1795.
[2] O. Hemeda, M. Barakat, Effect of hopping rate and jump length of hopping electrons on the conductivity and dielectric properties of Co–Cd ferrite, Journal of magnetism and magnetic materials, 223 (2001) 127-132.
[3] J. Tong, W. Li, L. Bo, H. Wang, Y. Hu, Z. Zhang, A. Mahboob, Selective oxidation of styrene catalyzed by cerium-doped cobalt ferrite nanocrystals with greatly enhanced catalytic performance, Journal of Catalysis, 344 (2016) 474-481.
[4] M. Amiri, M. Salavati-Niasari, A. Akbari, Magnetic nanocarriers: evolution of spinel ferrites for medical applications, Advances in colloid and interface science, 265 (2019) 29-44.
[5] K.C.B. Naidu, S.R. Kiran, W. Madhuri, Microwave processed NiMgZn ferrites for electromagnetic intereference shielding applications, IEEE Transactions Magnetics., 53 (2016) 1-7.
[6] H.R. Ebrahimi, H. Usefi, H. Emami, G.R. Amiri, Synthesis, characterization, and sensing performance investigation of copper cadmium ferrite nanoparticles, IEEE Transactions Magnetics., 54 (2018) 1-5.
[7] N. Chaibakhsh, Z. Moradi-Shoeili, Enzyme mimetic activities of spinel substituted nanoferrites (MFe_2O_4): A review of synthesis, mechanism and potential applications, Materials Science and Engineering: C, 99 (2019) 1424-1447.
[8] O. Opuchovic, G. Kreiza, J. Senvaitiene, K. Kazlauskas, A. Beganskiene, A. Kareiva, Sol-gel synthesis, characterization and application of selected sub-microsized lanthanide (Ce, Pr, Nd, Tb) ferrites, Dyes and Pigments, 118 (2015) 176-182.

[9] G. Mustafa, M. Islam, W. Zhang, Y. Jamil, A.W. Anwar, M. Hussain, M. Ahmad, Investigation of structural and magnetic properties of Ce^{3+}-substituted nanosized Co–Cr ferrites for a variety of applications, Journal of alloys and compounds, 618 (2015) 428-436.
[10] M. Rashad, S.M. Mahmoud, Z. Abdel-Hamid, H. El-Sayed, A.E. Shalan, N. Khalifa, A. Kandil, Structural, magnetic properties, and induction heating behavior studies of cobalt ferrite nanopowders synthesized using modified co-precipitation method, Particulate Science and Technology, 36 (2018) 172-177.
[11] A. Nikumbh, A. Nagawade, V. Tadke, P. Bakare, Electrical, magnetic and Mössbauer properties of cadmium-cobalt ferrites prepared by the tartarate precursor method, Journal of materials science, 36 (2001) 653-662.
[12] S. Bhongale, H. Ingawale, T. Shinde, K. Pubby, S.B. Narang, P. Vasambekar, Nano-crystalline magnesium substituted cadmium ferrites as X-band microwave absorbers, Journal of Magnetism and Magnetic Materials, 441 (2017) 475-481.
[13] E. Ateia, A.A. El-Bassuony, Fascinating improvement in physical properties of Cd/Co nanoferrites using different rare earth ions, Journal of Materials Science: Materials in Electronics, 28 (2017) 11482-11490.
[14] A.U. Rehman, N. Morley, N. Amin, M.I. Arshad, M.A. un Nabi, K. Mahmood, A. Ali, A. Aslam, A. Bibi, M.Z. Iqbal, Controllable synthesis of La^{3+} doped $Zn_{0.5}Co_{0.25}Cu_{0.25}Fe_{2-x}La_xO_4$ (x = 0.0, 0.0125, 0.025, 0.0375, 0.05) nano-ferrites by sol-gel auto-combustion route, Ceramics International, 46 (2020) 29297-29308.
[15] A. Aslam, A.U. Rehman, N. Amin, M. Amami, M. Nabi, H. Alrobei, M. Asghar, N. Morley, M. Akhtar, M.I. Arshad, Sol–Gel auto-combustion preparation of M^{2+}= Mg^{2+}, Mn^{2+}, Cd^{2+} substituted $M_{0.25}Ni_{0.15}Cu_{0.25}Co_{0.35}Fe_2O_4$ ferrites and their characterizations, Journal of Superconductivity and Novel Magnetism, 35 (2022) 473-483.
[16] P. Nayak, Synthesis and characterization of cadmium ferrite, Materials Chemistry and Physics, 112 (2008) 24-26.
[17] A.U. Rehman, S. Sharif, H. Hegazy, N. Morley, N. Amin, M. Akhtar, M.I. Arshad, Z. Farooq, Z. Munir, T. Munir, Low dielectric loss, and enhanced magneto-dielectric properties of $Cu_{0.5}Cd_{0.5-x}Co_xFe_2O_4$ ferrites via Co^{2+} substitution, Materials Today Communications, (2023) 105371.
[18] K. Hussain, N. Amin, M.I. Arshad, Evaluation of structural, optical, dielectric, electrical, and magnetic properties of Ce^{3+} doped $Cu_{0.5}Cd_{0.25}Co_{0.25}Fe_{2-x}O_4$ spinel nano-ferrites, Ceramics International, 47 (2021) 3401-3410.
[19] A. Aslam, A. Razzaq, S. Naz, N. Amin, M.I. Arshad, M. Nabi, A. Nawaz, K. Mahmood, A. Bibi, F. Iqbal, Impact of lanthanum-doping on the physical and electrical properties of cobalt ferrites, Journal of Superconductivity and Novel Magnetism, 34 (2021) 1855-1864.
[20] M.I. Arshad, M. Hasan, A.U. Rehman, M. Akhtar, N. Amin, K. Mahmood, A. Ali, T. Trakoolwilaiwan, N.T.K. Thanh, Structural, optical, electrical, dielectric, molecular vibrational and magnetic properties of La^{3+} doped Mg–Cd–Cu ferrites prepared by Co-precipitation technique, Ceramics International, 48 (2022) 14246-14260.
[21] S. Ahmad, S. Ali, I. Ullah, M. Zobaer, A. Albakri, T. Muhammad, Synthesis and characterization of manganese ferrite from low grade manganese ore through solid state reaction route, Scientific Reports, 11 (2021) 1-9.
[22] M.N. Akhtar, M.A. Khan, Effect of rare earth doping on the structural and magnetic features of nanocrystalline spinel ferrites prepared via sol gel route, Journal of Magnetism and Magnetic Materials, 460 (2018) 268-277.
[23] V. Vasanthi, A.Shanmugavani, C.Sanjeeviraja, R.KalaiSelvan, Microwave assisted combustion synthesis of $CdFe_2O_4$: Magnetic and electrical properties, Journal of Magnetism and Magnetic Materials, 324 (2012) 2100-2107.

[24] N. Amin, A. Razaq, A.U. Rehman, K. Hussain, M. Nabi, N. Morley, M. Amami, A. Bibi, M.I. Arshad, K. Mahmood, Transport Properties of Ce-Doped Cd Ferrites $CdFe_{2-x}Ce_xO_4$, Journal of Superconductivity and Novel Magnetism, (2021) 1-11.
[25] A.U. Rehman, N. Amin, M.B. Tahir, M.A. un Nabi, N. Morley, M. Alzaid, M. Amami, M. Akhtar, M.I. Arshad, Evaluation of spectral, optoelectrical, dielectric, magnetic, and morphological properties of RE^{3+} (La^{3+}, and Ce^{3+}) and Co^{2+} co-doped $Zn_{0.75}Cu_{0.25}Fe_2O_4$ ferrites, Materials Chemistry and Physics, (2021) 125301.
[26] R.R. Kanna, K. Sakthipandi, S.S.M.A. Maraikkayar, N. Lenin, M. Sivabharathy, Doping effect of rare-earth (lanthanum, neodymium and gadolinium) ions on structural, optical, dielectric and magnetic properties of copper nanoferrites, Journal of Rare Earths, 36 (2018) 1299-1309.
[27] M.I.U. Haq, M. Asghar, M.A.U. Nabi, N. Amin, S. Tahir, M.I. Arshad, Influence of Ce^{3+} and La^{3+} substitution on structural & optical parameters and electrical behavior on Mg-Zn ferrites synthesized via co-precipitation method, Journal of Superconductivity and Novel Magnetism, 35 (2022) 719-732.
[28] A. Aslam, A.U. Rehman, N. Amin, M.A. un Nabi, Q. ul ain Abdullah, N. Morley, M.I. Arshad, H.T. Ali, M. Yusuf, Z. Latif, Lanthanum doped $Zn_{0.5}Co_{0.5}La_xFe_{2-x}O_4$ spinel ferrites synthesized via co-precipitation route to evaluate structural, vibrational, electrical, optical, dielectric, and thermoelectric properties, Journal of Physics and Chemistry of Solids, 154 (2021) 110080.
[29] K. Patankar, D. Ghone, V. Mathe, S. Kaushik, Structural and physical property study of sol–gel synthesized $CoFe_{2-x}Ho_xO_4$ nano ferrites, Journal of Magnetism and Magnetic Materials, 454 (2018) 71-77.
[30] S.B. Somvanshi, S.A. Jadhav, M.V. Khedkar, P.B. Kharat, S. More, K. Jadhav, Structural, thermal, spectral, optical and surface analysis of rare earth metal ion (Gd^{3+}) doped mixed Zn–Mg nano-spinel ferrites, Ceramics International, 46 (2020) 13170-13179.
[31] M.F. Al-Hilli, S. Li, K.S. Kassim, Structural analysis, magnetic and electrical properties of samarium substituted lithium–nickel mixed ferrites, Journal of Magnetism and Magnetic Materials, 324 (2012) 873-879.
[32] A. Sinha, A. Dutta, Structural, optical, and electrical transport properties of some rare-earth-doped nickel ferrites: A study on effect of ionic radii of dopants, Journal of Physics and Chemistry of Solids, 145 (2020) 109534.
[33] A.U. Rehman, G. Abbas, B. Ayoub, N. Amin, M.A. un Nabi, N.A. Morley, M. Akhtar, M.I. Arshad, M.U. Khalid, M. Afzaal, Impact of Ni^{2+} on the structural, optical, electrical, and dielectric properties of $Cu_{0.25}Co_{0.25}Mg_{0.5-x}Ni_xCe_{0.03}Fe_{1.97}O_4$ spinel ferrites synthesized via sol-gel auto combustion (SGAC) route, Materials Science and Engineering: B, 291 (2023) 116407.
[34] S. Ikram, J. Jacob, K. Mehboob, K. Mahmood, N. Amin, M. Arshad, M. Ajaz un Nabi, Role of rare earth metal ions doping on structural, electrical, magnetic, and dielectric behavior of spinel ferrites: A comparative study, Journal of Superconductivity and Novel Magnetism, 34 (2021) 1833-1842.
[35] M. Hashim, M. Raghasudha, S.S. Meena, J. Shah, S.E. Shirsath, S. Kumar, D. Ravinder, P. Bhatt, R. Kumar, R. Kotnala, Influence of rare earth ion doping (Ce and Dy) on electrical and magnetic properties of cobalt ferrites, Journal of Magnetism and Magnetic Materials, 449 (2018) 319-327.
[36] B.P. Jacob, S. Thankachan, S. Xavier, E. Mohammed, Dielectric behavior and AC conductivity of Tb^{3+} doped $Ni_{0.4}Zn_{0.6}Fe_2O_4$ nanoparticles, Journal of Alloys and Compounds, 541 (2012) 29-35.
[37] M. Ajmal, M.U. Islam, G.A. Ashraf, M.A. Nazir, M. Ghouri, The influence of Ga doping on structural magnetic and dielectric properties of $NiCr_{0.2}Fe_{1.8}O_4$ spinel ferrite, Physica B: Condensed Matter, 526 (2017) 149-154.

[38] M. Farid, I. Ahmad, G. Murtaza, M. Kanwal, I. Ali, Electric modulus properties of praseodymium substituted copper ferrites, Journal of Ovonic Research, 12 (2016), 137-146.

Table 1 Lattice parameters of Ce-CF samples

Parameters	$x = 0.0$	$x = 0.02$	$x = 0.04$	$x = 0.06$	$x = 0.08$	$x = 0.1$
a (Å)	8.675	8.690	8.720	8.871	8.750	8.679
V (Å^3)	652	656	663	698	671	653
D (nm)	40	45	36	34	27	25
ρ_x (g/cm^3)	5.863	5.862	5.84	5.57	5.83	6.02
ρ_m (g/cm^3)	1.23	0.87	0.76	0.65	0.74	0.88
P (%)	78	85	86	88	87	85
L_A (nm)	0.375	0.376	0.377	0.384	0.379	0.375
L_B (nm)	0.306	0.307	0.308	0.313	0.309	0.306
δ (nm^{-2})	0.000607	0.000491	0.000686	0.001043	0.001062	0.001315

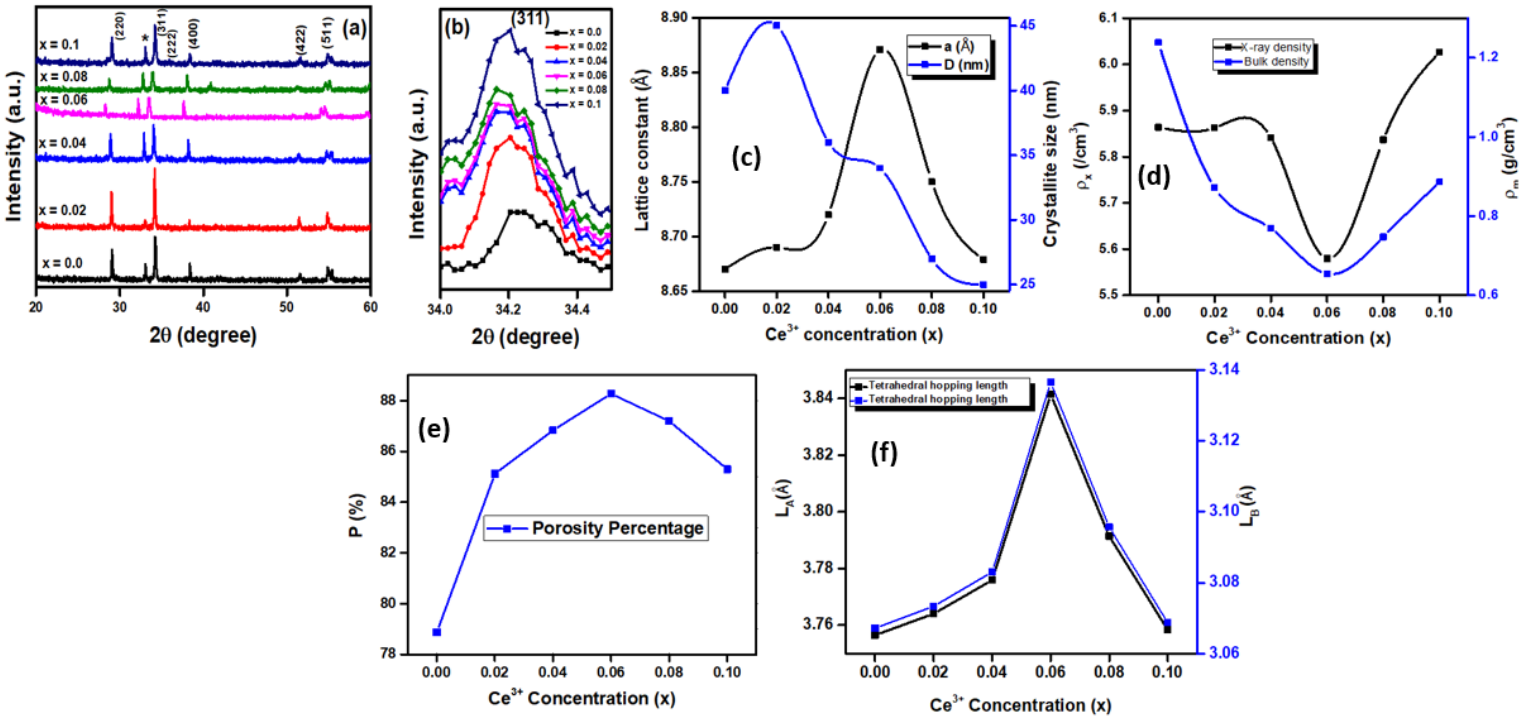

Fig. 1(a) XRD pattern for Ce-CF samples **(b)** peak (311) shift for all the samples **(c)** lattice constant and crystallite size *versus* Ce^{3+} concentration **(d)** Variation in X-ray density (ρ_x) and bulk density (ρ_m) with dopant concentration **(e)** *P* (%) *versus* Ce^{3+} concentration **(f)** hopping length *A* and *B* sites *versus* Ce^{3+} concentration

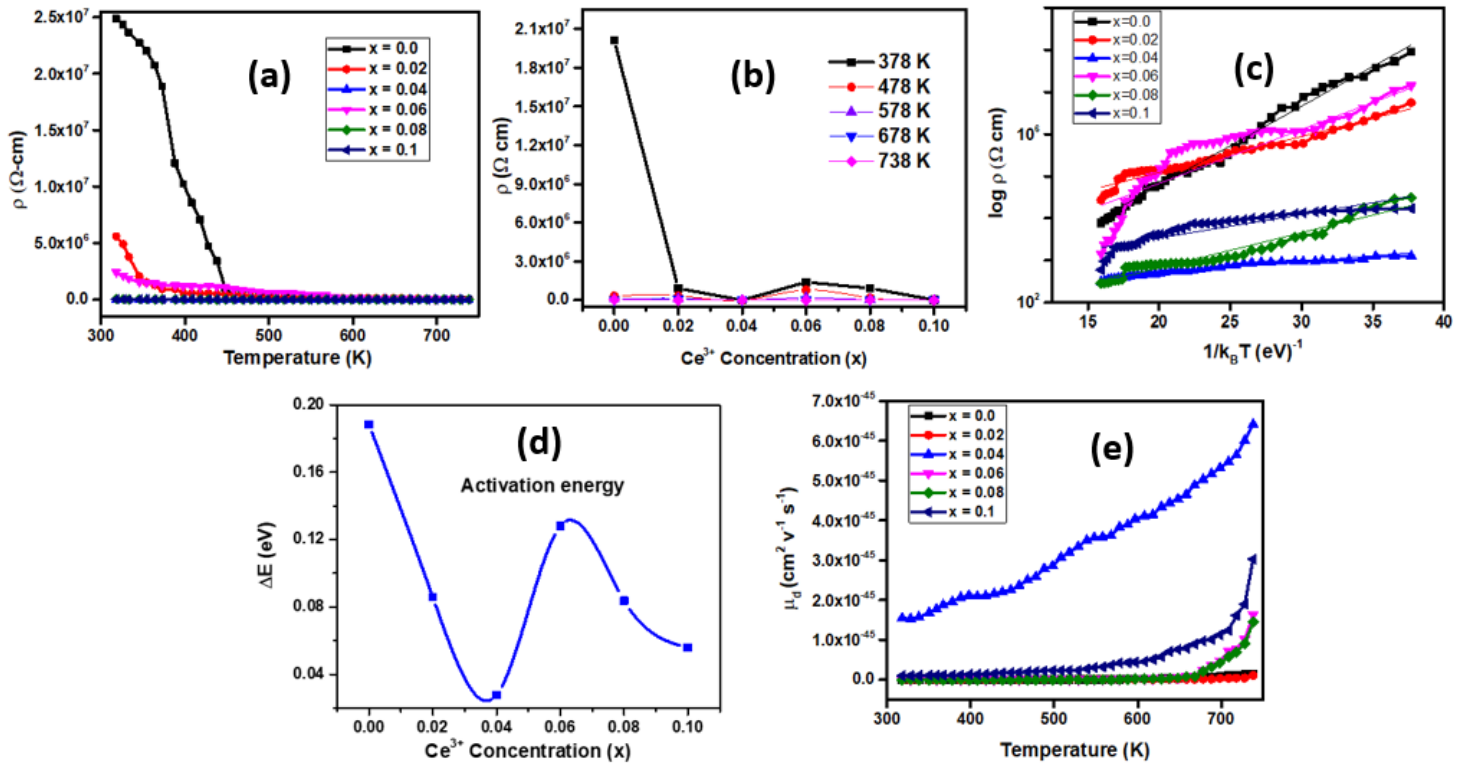

Fig. 2(a) Variation in DC resistivity (ρ) with temperature **(b)** resistivity *versus* Ce^{3+} concentration at different temperatures **(c)** Plots of the log of DC resistivity *versus* $1/k_BT$ **(d)** Effect of Ce^{3+} concentration (x) on the activation energy for $CdCe_xFe_{2-x}O_4$ **(e)** Variation of drift mobility (μ_d) with temperature (T)

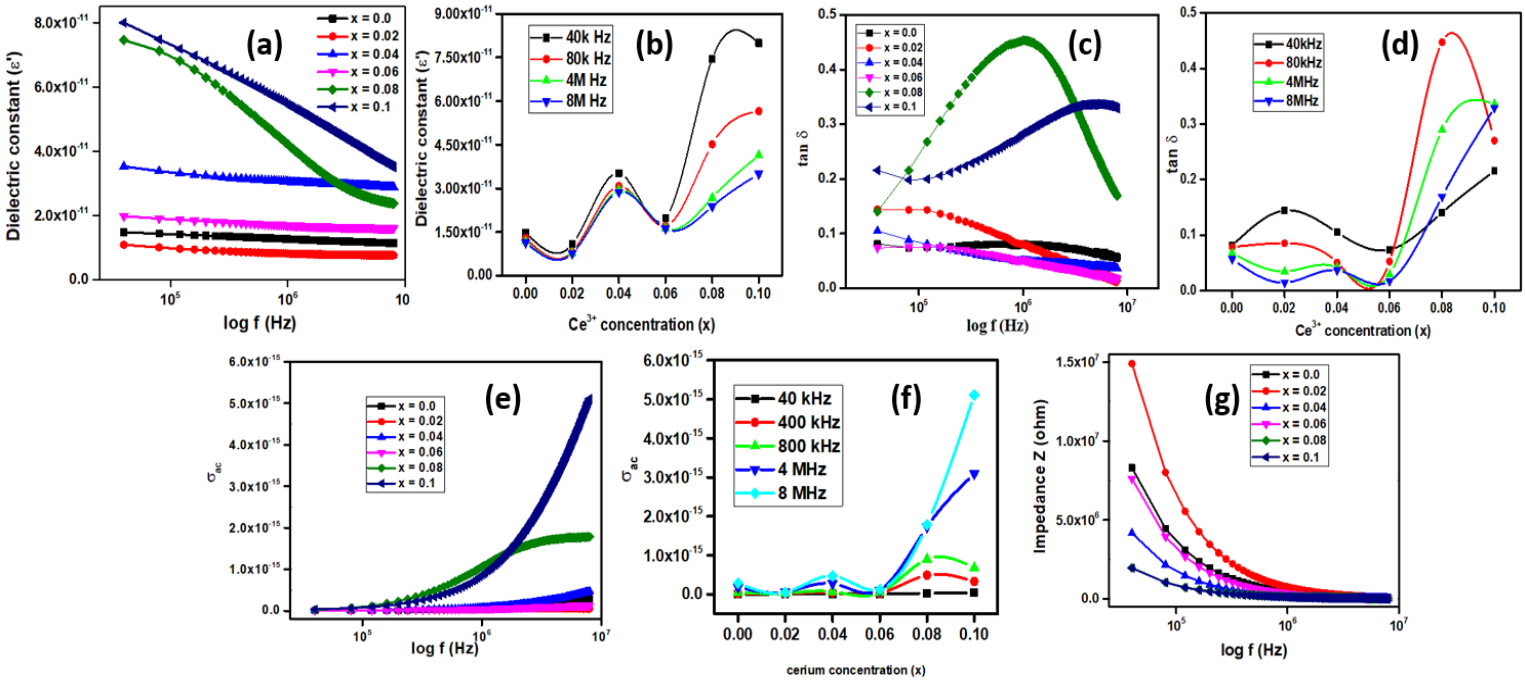

Fig. 3(a) Dielectric constant *versus* log f **(b)** Effect of Ce^{3+} concentration on the dielectric constant **(c)** Plots of dielectric tangent loss *versus* log f **(d)** Effects of Ce^{3+} concentration on dielectric loss at different frequencies **(e)** Plots of ac conductivity *versus* log f **(f)** Effect of Ce^{3+} concentration on ac conductivity **(g)** Variation in impedance with a log of frequency for Ce-CF samples

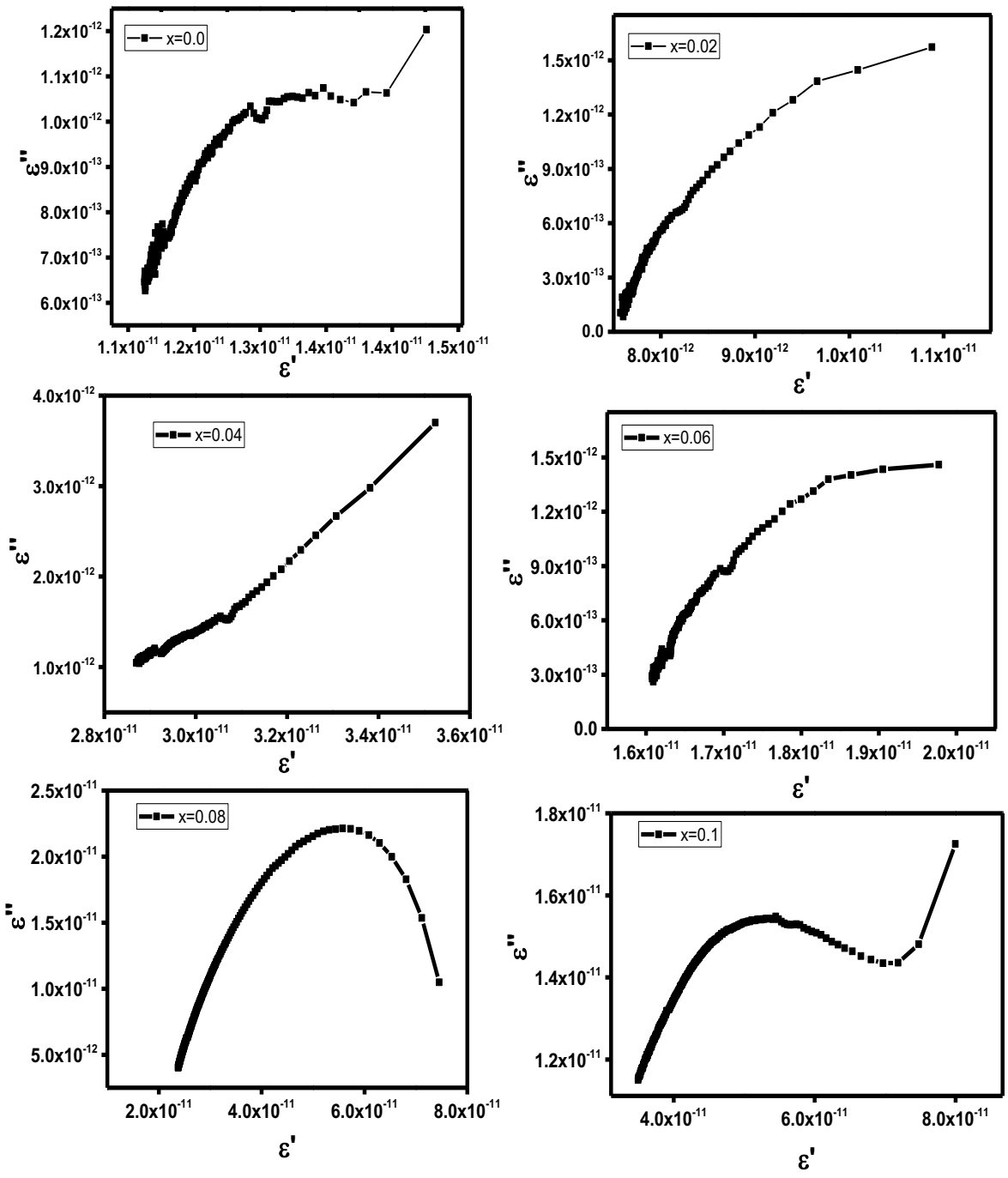

Fig. 4 Cole-Cole plots for Ce-CF samples